Available online at www.sciencedirect.com
SCIENCE DIRECT®
Journal of the European Ceramic Society 25 (2005) 473–480
www.elsevier.com/locate/jeurceramsoc

Sinterability, microstructures and electrical properties of Ni/Sm-doped ceria cermet processed with nanometer-sized particles

Yoshihiro Okawa, Yoshihiro Hirata*

Department of Advanced Nanostructured Materials Science and Technology, Graduate School of Science and Engineering, Kagoshima University 1-21-40 Korimoto, Kagoshima 890-0065, Japan

Received 1 July 2003; received in revised form 19 January 2004; accepted 25 January 2004
Available online 21 July 2004

Abstract

Ni/Sm-doped ceria (SDC) cermet was prepared from two types of NiO/SDC mixed powders: Type A—Mechanical mixing of NiO and SDC powders of micrometer-sized porous secondary particles containing loosely packed nanometer-sized primary particles. The starting powders were synthesized by calcining the oxalate precursor formed by adding the mixed nitrate solution of Ce and Sm or Ni nitrate solution into oxalic acid solution. Type B—Infiltration of $Ni(NO_3)_2$ solution into the SDC porous secondary particles subsequently freeze-dried. Type B powder gave denser NiO/SDC secondary particles with higher specific surface area than Type A powder. The above two types powders were sintered in air at 1100–1300 °C and annealed in the H_2/Ar or H_2/H_2O atmosphere at 400–700 °C. Increased NiO content reduced the sinterability of Type A powder but the bulk density of Type B powder compact showed a maximum at 34 vol.% NiO (25 vol.% Ni). Type B cermet was superior to Type A cermet in achieving fine-grained microstructure and a homogeneous distribution of Ni and SDC grains. The electrical resistance of the produced cermet decreased drastically at 15 vol.% Ni for Type B and at 20 vol.% Ni for Type A.

Keywords: Sintering; Nanocomposites; Electrical conductivity; Fuel cells; CeO_2

1. Introduction

In the past two decades, solid oxide fuel cells (SOFCs) have been studied intensively because of advantages such as high energy conversion, little air pollution, no loss of solid electrolyte and utilization of high temperature exhaust gas. Such cells are composed of solid electrolyte, anode, cathode and interconnector. In the anode, oxide ions supplied from the solid electrolyte react with H_2 gas to produce electrons. An extensive triple phase boundary (TPB), the intersection of the solid electrolyte-electronic conductor-H_2 gas phases, leads to high electric power. A metal/ceramic composite (cermet) acting as a mixed conductor of electrons and oxide ions forms an advantageous anode material of SOFC. The following candidate cermet materials have been proposed: Ni/Y_2O_3-stabilized ZrO_2 (YSZ),[1–5] Ru/Sm-doped ceria (SDC),[6] Ni/CeO_2,[7] Ni/Gd-doped ceria (GDC),[8] and Ni/SDC.[9–12] The important functions of the YSZ particles in the Ni/YSZ cermet are to: (1) supply oxide ions to the TPB,[4] (2) suppress the sintering of Ni, and (3) match the thermal expansion coefficients between the cermet and the YSZ electrolyte. The electrical properties of the cermet depend on its microstructure. Ni particles in the Ni/YSZ cermet should be connected to YSZ particles (oxide ion supplier) and also exposed to H_2 gas. The electrical conductivity of Ni/YSZ cermet increases about 3 orders of magnitude at Ni contents above 30 vol.% on the basis of a percolation model.[1] The Ni/YSZ cermet is usually made from YSZ and NiO mixed powders. The mixed powders are deposited or printed on a solid electrolyte and heated to make a porous structure over 1100 °C, and then exposed to a hydrogen gas to reduce NiO to Ni metal. The prevention of sintering of the Ni particles during long-term operation of SOFC at 700–1000 °C should be controlled to maintain the extensive TPB.

The degradation of cell performance is mainly caused by the following problems under long-term operation of SOFC: (1) the decrease in the active surface of the Ni particles[1] and (2) formation of cracks in the anode close to the anode/electrolyte interface. To solve the above problem (1), a Ni/YSZ cermet with high thermal stability was made by the

* Corresponding author. Tel.: +81-99-285-8325; fax: +81-99-257-4742.
E-mail address: hirata@apc.kagoshima-u.ac.jp (Y. Hirata).

0955-2219/$ – see front matter © 2004 Elsevier Ltd. All rights reserved.
doi:10.1016/j.jeurceramsoc.2004.01.011

optimization of the particle size distribution of YSZ and Ni phases. A decrease in the size of the Ni particles significantly decreases the anode resistance because of the increased length of the TPB. According to Jiang et al.[2] a fine YSZ powder of narrow particle size distribution of 0.06–0.1 μm and submicrometer-sized Ni powder (∼0.2 μm) with broad particle size distribution are beneficial for the formation of the YSZ-to-YSZ and Ni-to-Ni networks. Recently, a Ni/rare-earth-doped ceria cermet has been investigated because of the enhanced reaction area due to the electrical property of the mixed conductor. Eguchi and coworkers prepared a cermet anode from micrometer-sized Ni and Sm-doped ceria powders.[7,11] Livermore et al.[8] observed two types of Ni particles in a commercial NiO/GDC composite after reduction by methane reforming: large "bulk" Ni particles and smaller Ni particles in intimate contact with GDC. The stability of the porous structure of the composite is dominated by the large "bulk" Ni particles while the smaller Ni particles contribute to increase the length of the TPB formed in the GDC-Ni-fuel gas system. That is, the suppression of sintering of fine solid electrolyte and Ni particles during the operation of the SOFC is a key factor to provide a high performance anode. The second problem (2) results from the difference of thermal expansion coefficients between anode and solid electrolyte. Decrease of the Ni content in the Ni/YSZ or Ni/SDC cermet is effective to reduce the difference of the thermal expansion coefficient. However, a too small Ni content results in the disappearance of electronic conduction. For the solution to both the problems (1) and (2), the following cermet structure is proposed: larger solid electrolyte particles are connected to each other to make a porous structure, because the sinterability of the electrolyte powder is lower than that of Ni metal at the operation temperature of the SOFC. Smaller Ni particles are at the same time deposited on the surface of the electrolyte particles, like a continuous network, to increase the length of the TPB. In this experiment, two types of Ni/SDC cermet were prepared: Type A—Mechanically mixed cermet consisting of micrometer-sized secondary SDC and NiO powders. In the porous secondary SDC and NiO powders, the nanometer-sized primary particles were packed loosely. The mixed cermet powder was sintered at 1100–1300 °C in air. Type B—An aqueous $Ni(NO_3)_2$ solution was infiltrated into the pores in the porous secondary SDC powder and the suspension of $Ni(NO_3)_2$-SDC powder system was freeze-dried and then sintered at 1300 °C in air. This paper reports on the sinterability, microstructures and electrical properties of these two types of cermet.

2. Experimental procedure

2.1. Processing of Ni/SDC cermet

2.1.1. Type A

The fabrication process of the Ni/SDC cermet of Type A is shown in Fig. 1. The detailed powder preparation method of Sm-doped ceria with a composition of $Ce_{0.8}Sm_{0.2}O_{1.9}$

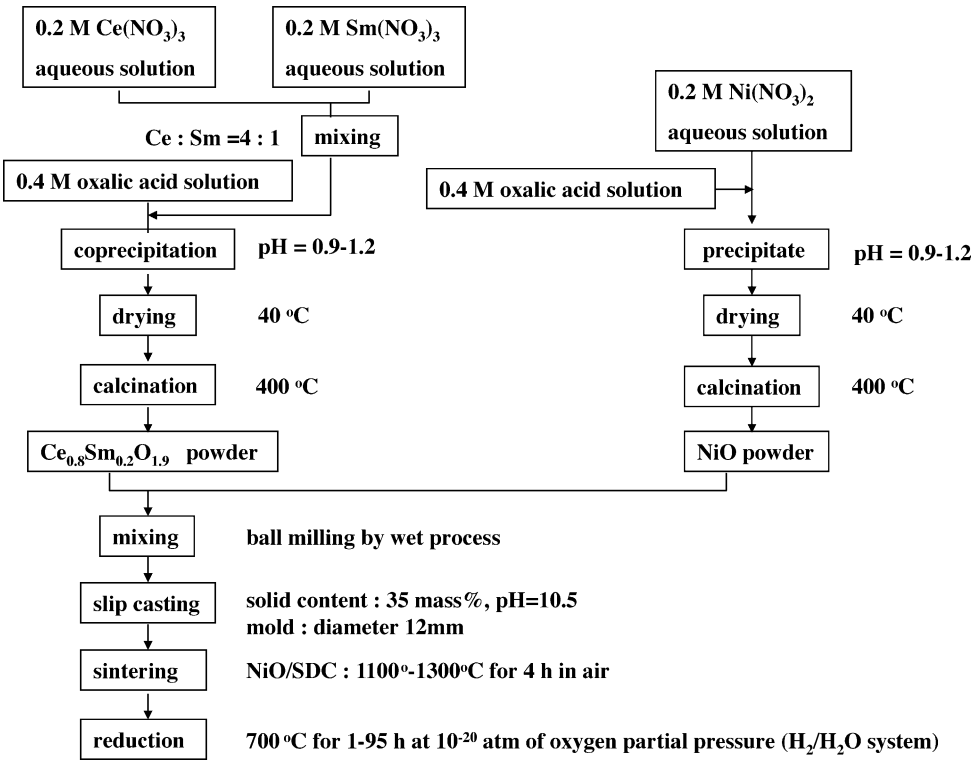

Fig. 1. Flow chart for the preparation of Ni/Sm-doped ceria cermet of Type A.

and NiO are reported in our previous papers.[13–15] The oxalate solid solution $(Ce_{0.8}Sm_{0.2})_2(C_2O_4)_3$ was produced at room temperature by adding the mixed nitrate solution (0.2 M) of Ce and Sm into 0.4 M oxalic acid solution. The coprecipitated oxalate powder decomposed to polycrystalline oxide solid solution upon heating to 400–600 °C. The SDC powder was observed with transmission electron microscopy (H-700, Hitachi Co., Tokyo, Japan). In parallel, a fine NiO powder was produced from nickel oxalate NiC_2O_4. $Ni(NO_3)_2$ (0.2 M) solution was added into 0.4 M oxalic acid solution and aged for 120 h at room temperature. The produced NiC_2O_4 was vacuum-filtered, washed with distilled water and dried at 40 °C overnight and then calcined in a platinum crucible at 400–600 °C in air. These calcined powders were mixed by wet ball-milling with zirconia balls (diameter 3 mm) in a polyethylene bottle for 20 h. The size of the milled powder was measured with a particle size distribution analyzer (CAPA-700, Horiba Co., Japan). The mixed powder suspension with solid content of 35 vol.% at pH 10.5 was cast in gypsum molds (diameter 12 mm). After drying at 40 °C for 20 h, the green compacts were sintered at 1100–1300 °C in air (SPM6512 electric furnace, Marusho Electro-Heat Co., Ltd., Japan). The sintered sample was annealed in a H_2/H_2O atmosphere of oxygen partial pressure of 10^{-20} atm at 700 °C for 1–95 h. The oxygen partial pressure of the H_2/H_2O system was monitored with a YSZ oxygen sensor (KOA-200, Kaken Inc., Ibaraki, Japan).

2.1.2. Type B

The fabrication process of 5–45 vol.% Ni/SDC cermet of Type B is shown in Fig. 2. The SDC powder with a composition of $Ce_{0.8}Sm_{0.2}O_{1.9}$ was prepared by calcining the precursor oxalate solid solution at 400 °C. This powder was immersed in 1.4 M $Ni(NO_3)_2$ solution and freeze-dried (FRD-50 M Freeze Dryer, Iwaki Glass Co., Ltd., Japan). The dried SDC powder containing $Ni(NO_3)_2$ was heated at 350 °C for 1 h in air and formed by uniaxial dry pressing at 100 MPa to a pellet of 10 mm diameter and 2 mm thickness. The structure of the calcined composite powder was observed by transmission electron microscopy (H-700, Hitachi Co.). The green compact was sintered at 1300 °C for 4 h in air. The sintered composite was annealed in a H_2/H_2O atmosphere of 10^{-20} atm oxygen partial pressure at 700 °C. The NiO/SDC composite powder calcined at 350 °C was heated further at 400–800 °C for 1 h to measure the specific surface area by the BET method (FlowsorbII 2300, Shimazu Co., Kyoto, Japan).

2.2. Evaluation of physical properties and microstructure of Ni/SDC cermet

The bulk density and porosity of the Ni/SDC cermet before and after the reduction were measured by the Archimedes method using distilled water. The theoretical density of SDC and NiO were calculated from their lattice parameters. The crystalline phases of the Ni/SDC cermet after the reduction were identified by X-ray diffraction (Cu Kα, Model No. 2013, Rigaku Co., Japan). The distribution of Ni, Ce, and Sm elements in the Ni/Sm cermet after the reduction was evaluated by electron probe microanalyzer (EMX-SM7, Shimadzu Co., Kyoto, Japan). The Ni/SDC cermet annealed in a H_2/H_2O atmosphere at 700 °C was characterized by BET surface area measurement (Flowsorb II 2300, Shimadzu Co.) and scanning electron microscope (SM-300, Topcon Co., Japan).

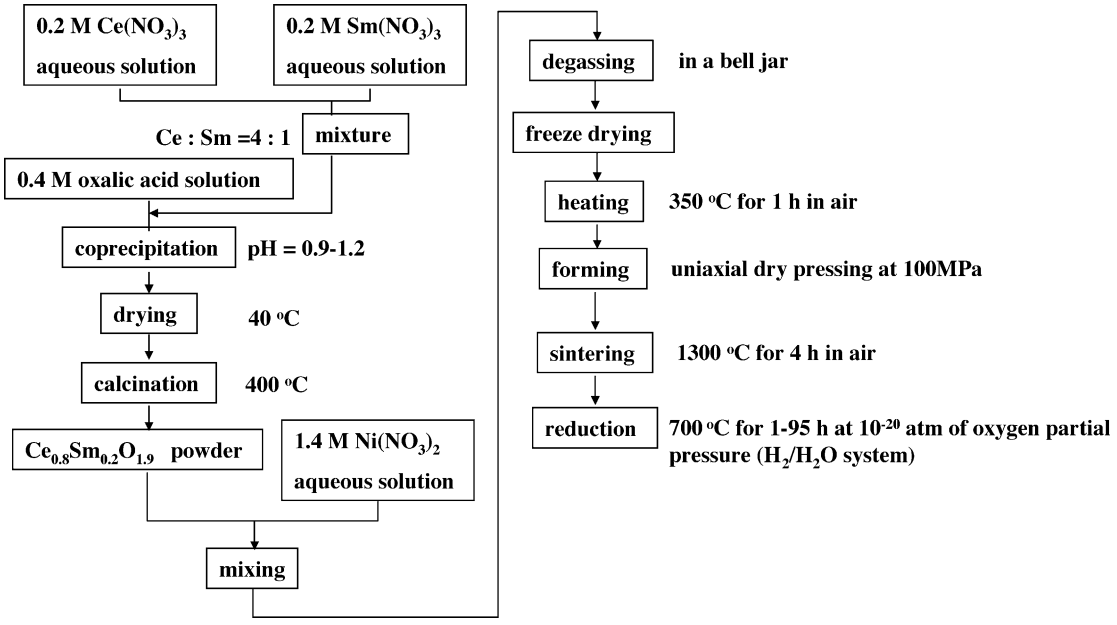

Fig. 2. Flow chart for the preparation of Ni/SDC cermet of Type B.

2.3. Measurement of electrical properties of Ni/SDC cermet

The electrical resistance of the Ni/SDC cermet after the reduction was measured at 700 °C in a H_2/H_2O atmosphere of oxygen partial pressure of 10^{-20} atm. Au thin film of 30 nm thickness was sputtered on the polished planes of a Ni/SDC pellet. Electrical contact was made via Pt plates with Pt lead wire under pressurized contact with the Au electrodes. The electrical resistance of the Ni/SDC cermet was measured by potentiometer (HA-501G, Hokuto Denko Co., Tokyo, Japan).

3. Results and discussion

3.1. Characteristics of NiO/SDC powder

Fig. 3a and b shows the specific surface area and the diameter of an equivalent spherical particle for the SDC and NiO powders (Type A) calcined at 400–800 °C, respectively. The result in Fig. 3 and observation of the calcined powders by transmission electron microscope indicated that the increase in the calcination temperature caused the disappearance of fine nanometer-sized pores formed between primary particles and grain growth of the primary particles within the secondary particles. The size of the secondary particles of SDC powder after the calcination at 400–600 °C, measured by particle size analyzer in dilute aqueous suspension, was 1.9–2.3 μm. The NiO powder had a lower specific surface area than the SDC powder. The secondary particle size of NiO calcined at 400 and 600 °C was 1.8 μm. Fig. 4 shows the specific surface area and the diameter of the equivalent spherical particle of Type B powder containing 7.8, 21.9,

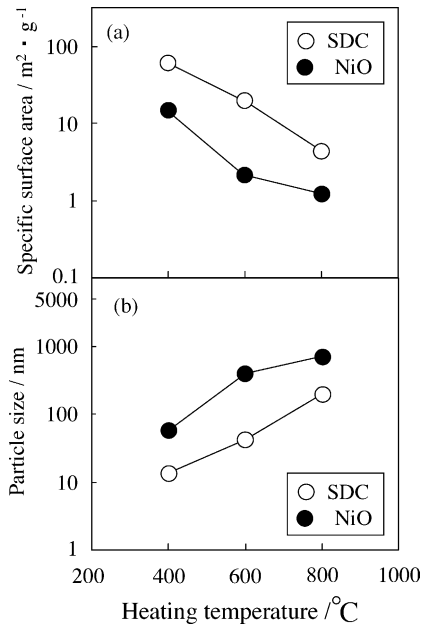

Fig. 3. (a) Specific surface area and (b) diameter of an equivalent spherical particle for SDC and NiO precursors calcined at 400–800 °C.

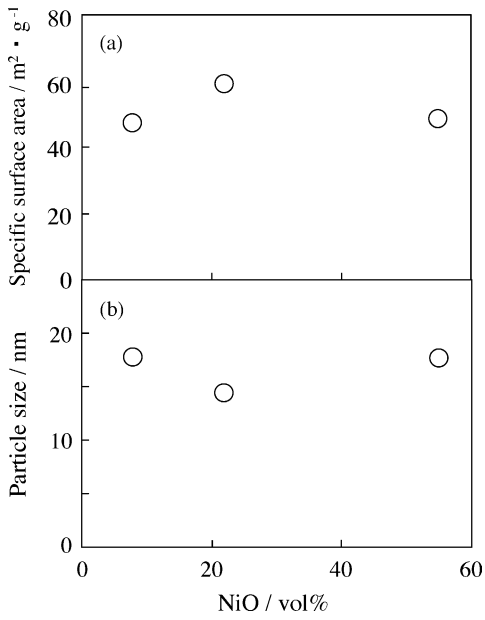

Fig. 4. (a) Specific surface area and (b) diameter of an equivalent spherical particle of Type B powder calcined at 350 °C in air, as a function of NiO content.

and 54.9 vol.% NiO, calcined at 350 °C for 1 h in air. The specific surface area of Type B powder was not sensitive to the NiO content. The structure of Type B powder with 7.8 vol.% NiO, observed by transmission electron microscope, was denser than that of Type A powder without the NiO component. That is, Type B powder produces dense secondary particles with high specific surface area because of the low reactivity between the nanometer-sized SDC and the NiO primary particles. Furthermore, the observation of Type B powder by transmission electron microscope indicated that the increase of the NiO content was accompanied by decrease of the secondary particle size. This observation explains no decrease of the specific surface area of Type B powder with increased NiO content.

Fig. 5 shows the specific surface area of NiO/SDC mixed powder heated at 400, 600, and 800 °C for 1 h in air. In Fig. 5, the specific surface area calculated by mixing rule, is also presented. The Type B powder calcined at 350 °C for 1 h in air after freeze-drying (Fig. 2), was further heated at 400–800 °C for 1 h. The measured specific surface areas of Type A powder for two compositions in Fig. 5 were larger than the calculated ones at the low heating temperature of 400 °C, suggesting that mass transport in the mixed system was suppressed relative to that in the separate systems. However, no difference in the specific surface areas was observed between the measurement and calculation for Type A calcined at 600 and 800 °C, suggesting that no significant impediment in the mixed powder for sintering/grain growth. On the other hand, the specific surface area of Type B powder was two or three-times as high as that of Type A powder. In addition, the specific surface area of Type B powder became higher at higher content of NiO. This tendency of

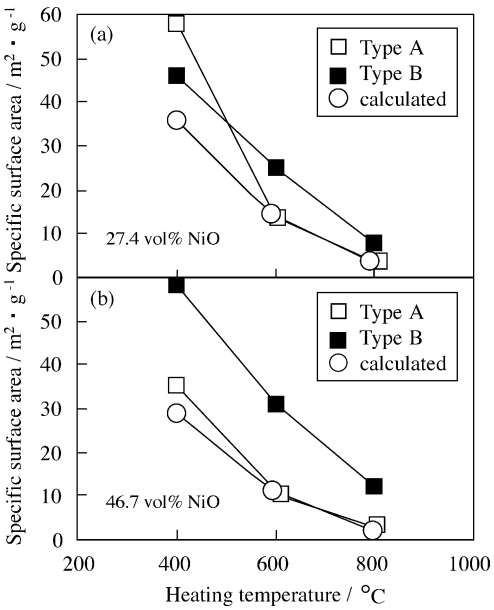

Fig. 5. Influence of heating temperature on specific surface areas of NiO/SDC mixed powders with (a) 27.4 and (b) 46.7 vol.% NiO. Some specific surface areas calculated by mixing rule are also presented.

Type B powder was opposite to that of Type A powder. That is, the mixing of chemically compatible oxides at nanometer scale can keep a high specific surface area after the heat treatment at 400–800 °C.

3.2. Sintering behavior of Ni/SDC cermet

Fig. 6 shows the fractions of (a) solid, (b) open pore, and (c) closed pore of the NiO/SDC compact (Type A) after the annealing in the H_2/Ar atmosphere at 400 °C. The starting NiO and SDC powders were calcined at 400 °C before the sintering and sintered at 1100–1300 °C in air. The NiO component in the sintered compact was reduced to Ni after the annealing in the H_2/Ar atmosphere. The increase of NiO content in the mixed powder compact reduced the sinterability. Although the porosity of closed pore of Type A cermet was almost independent of NiO content and sintering temperature, the fraction of open pore decreased by the sintering at a higher temperature. The similar result was also measured for the powder compact formed from the NiO and SDC powders calcined at 600 °C before sintering. On the other hand, the sintering behavior of Type B powder was different from that of Type A powder. Fig. 6 also shows the relative density and porosity of sintered Type B compact after the reduction of NiO to Ni. The porosity of open pore decreased with increasing Ni content and showed a minimum at about 25 vol.% Ni. On the other hand, the porosity of closed pore increased with increasing Ni content and showed a maximum at 45 vol.% Ni.

Fig. 7 shows the relative density and porosity of powder compacts of Types A and B with 54.9 vol.% NiO as a function of annealing time (1–95 h) in a H_2/H_2O atmosphere

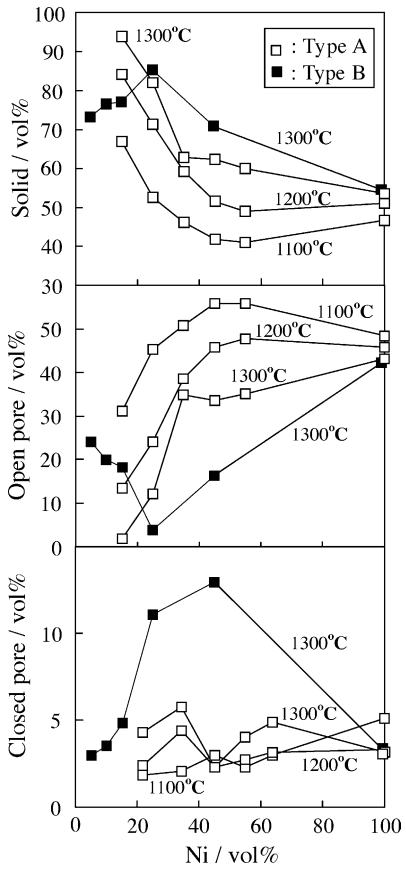

Fig. 6. Fractions of solid and pores of the Ni/SDC cermet annealed at 400 °C in a 25% H_2/75% Ar atmosphere after the sintering at 1300 °C for 4 h in air.

with oxygen partial pressure of 2×10^{-20} to 8×10^{-20} atm at 700 °C. The starting Types A and B compacts were sintered at 1300 °C for 4 h in air. Type A compact showed no significant change in relative density or porosity during the annealing period of 1–95 h, indicating the rapid reduction of the NiO component to Ni in the NiO/SDC compact with high porosity of open pore. As compared with Type A compact, the NiO component in Type B powder compact was more gradually reduced to Ni. After 24 h of the annealing, the porosity of open and closed pores reached constant values as seen in Fig. 7b and c. The specific surface areas of Types A and B compacts after the annealing for 1, 10, and 95 h at 700 °C were as follows: 0.54, 0.66, and 0.59 m^2/g for the Type A compact, and 0.51, 0.79, and 0.70 m^2/g for the Type B compact. These values were much smaller than the specific surface areas of Types A and B powders before the sintering in air (Fig. 3). The sintering of Types A and B powders in air caused the drastic decrease in the specific surface area (<1 m^2/g).

3.3. Microstructure of Ni/SDC cermet

Fig. 8 shows the microstructures of (a) Type A compact with 54.9 vol.% NiO, sintered at 1300 °C in air, and

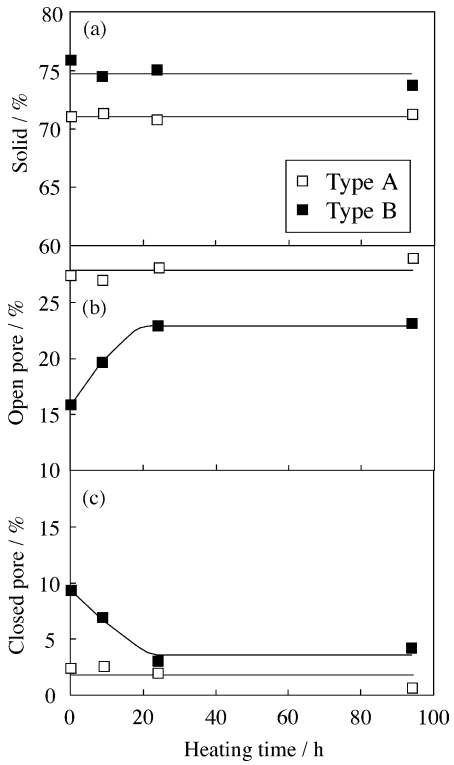

Fig. 7. Relative density and porosity of sintered Types A and B compacts with 54.9 vol.% NiO as a function annealing time in the H_2/H_2O atmosphere of oxygen partial pressure of 10^{-20} atm at 700 °C.

Type A Ni/SDC cermet annealed at 700 °C in the H_2/H_2O atmosphere of oxygen partial pressure of 10^{-20} atm for (b) 1 h, (c) 10 h, and (d) 95 h. As-sintered NiO/SDC compact with 78.4% relative density consisted of equiaxes grains of 0.5–1.6 μm. The annealing of the NiO/SDC compact in the low oxygen partial pressure formed open pores due to the reduction of NiO to Ni. The increase of the annealing time gave a small influence on the porosity of open and closed pores, as seen in Fig. 7. The change in the microstructure was not significant as the annealing time increased. Fig. 9a shows the microstructure of Type B compact with 54.9 vol.% NiO, sintered at 1300 °C. The grain size of as-sintered compact with 85.3% relative density was in the range from 0.2 to 1.0 μm and smaller than that of Type A compact. The annealing of Type B compact in the H_2/H_2O atmosphere at 700 °C gradually increased the porosity of open pore (Fig. 7). After 95 h of the annealing, Type B cermet still showed a fine-grained microstructure (Fig. 9d). The distribution of Ni, Ce, and Sm elements in Types A and B cermet with 45 vol.% Ni, annealed at 700 °C for 24 h in the H_2/H_2O atmosphere, were examined by electron probe microanalyzer. In Type A, Ni and SDC grains were mixed at intervals of 1–3 μm. The Sm was well dissolved in CeO_2 matrix. As compared with Type A cermet, a more homogeneous distribution of Ni and SDC grains was measured in Type B cermet. The above results are coupled to lead to the conclusion that Type B cermet is superior to Type A cermet in achieving the high relative density, fine-grained microstructure and homogeneous distribution of Ni and SDC particles.

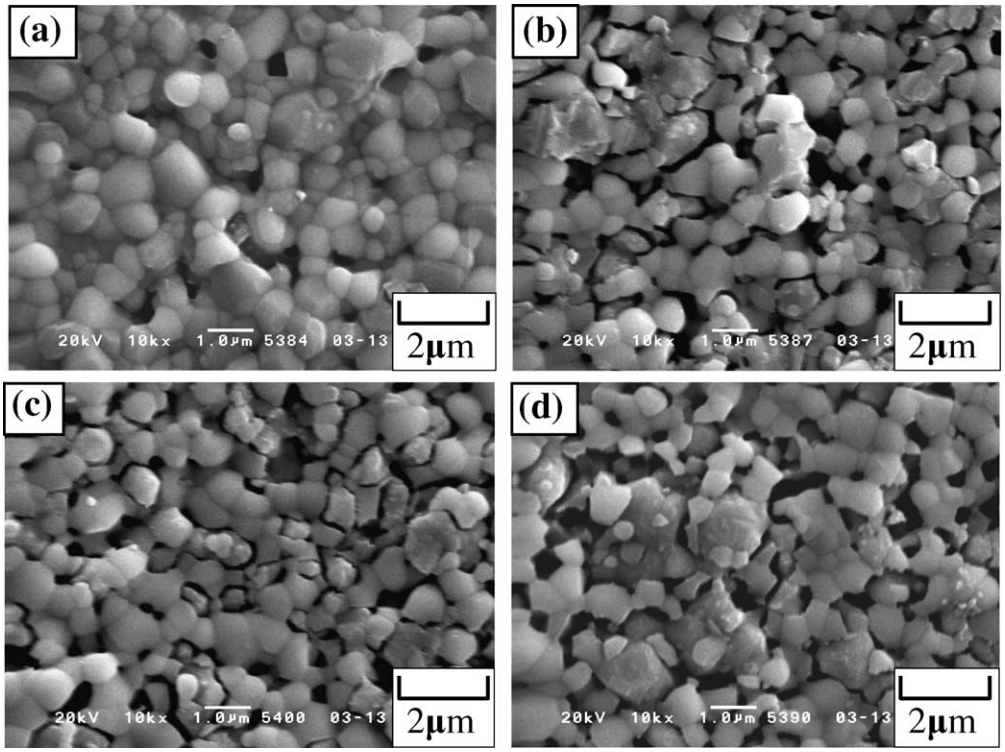

Fig. 8. Microstructures of (a) sintered Type A compact with 54.9 vol.% NiO and Type A cermet annealed at 700 °C in the H_2/H_2O atmosphere for (b) 1, (c) 10, and (d) 95 h.

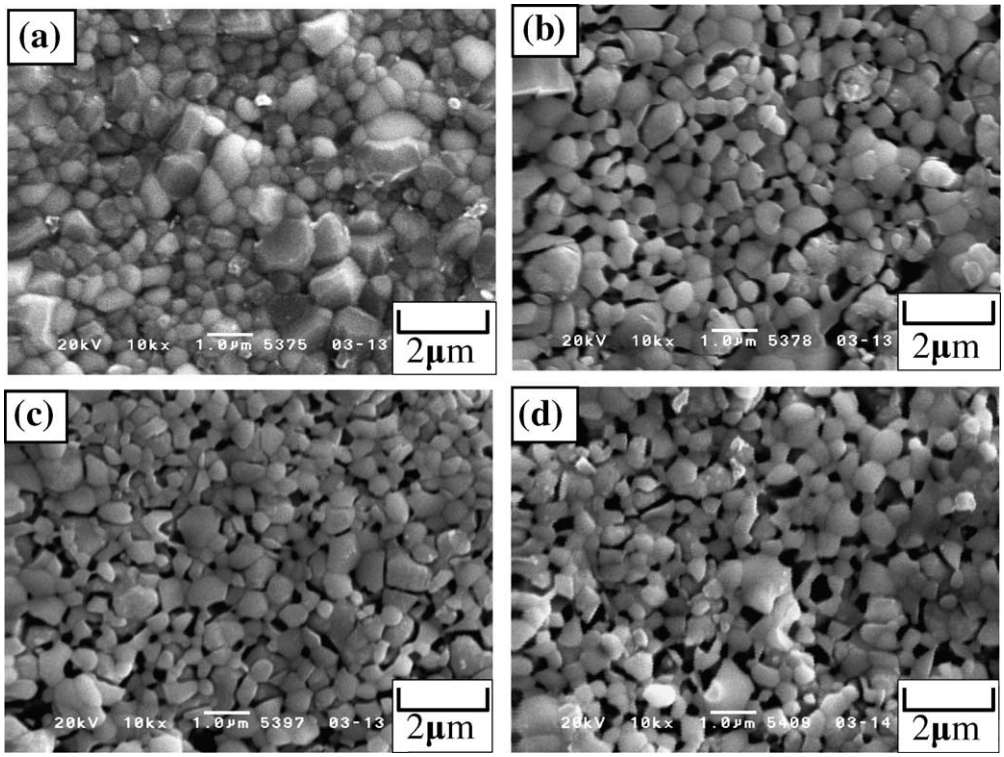

Fig. 9. Microstructures of (a) Type B compact with 54.9 vol.% NiO and Type B cermet annealed in the H_2/H_2O atmosphere at 700 °C for (b) 1, (c) 10, and (d) 95 h.

3.4. Electrical properties of the Ni/SDC cermet

Fig. 10 shows the comparison of the resistance of Types A and B cermet measured in the H_2/H_2O atmosphere at 700 °C after annealing for 24 h. The samples were sintered in air at 1300 °C before the electrical conductivity measurement. In this experiment, it was difficult to separate the measured resistance into the accurate resistance of Ni/SDC cermet and Pt plate/Pt lead wire because of too small values of measured resistance. The data presented in Fig. 10 included both the resistance of Ni/SDC cermet and Pt electrodes. In the Ni content range from 25 to 55 vol.%, a low constant resistance was measured for the Type A cermet. When the Type A sample with 45 vol.% Ni was heated in the H_2/H_2O atmosphere for 1–95 h, no increase of the electrical resistance was measured, indicating the stable electrical characteristic of Type A cermet. On the other hand, Type B cermet showed a lower resistance at 15 vol.% Ni than Type A cermet. At the Ni content higher than 25 vol.%, no difference of electrical resistance was measured between Types A and B cermet. In addition, the high stability of the low electrical resistance was also measured on Type B cermet heated at 700 °C for 1–95 h in the H_2/H_2O atmosphere. Various percolation models are proposed to explain the sudden change in the electrical conductivity of two phase systems.[16–23] In this paper, we modified the Fermi–Dirac distribution which gives the probability that an orbital at certain energy will be occupied in an electron gas in thermal equilibrium. Eq. (1) represents the conductivity of two phases system

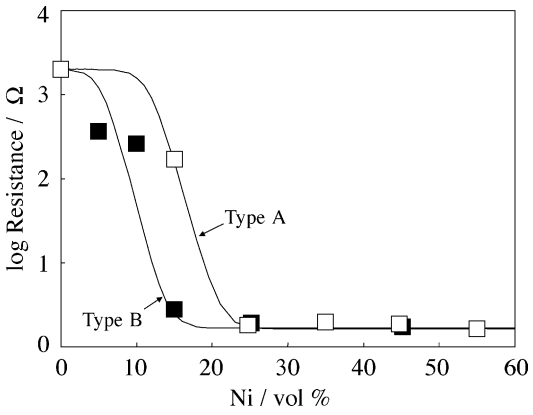

Fig. 10. Comparison of electrical resistance of Types A and B cermet measured in the H_2/H_2O atmosphere of oxygen partial pressure of 10^{-20} atm at 700 °C after annealing for 24 h. The solid lines in this figure represent Eq. (1) in text.

$$\sigma = \sigma_0 + \frac{\sigma_1 - \sigma_0}{1 + \exp\left((V_C - V/n)\right)} \quad (1)$$

where σ_0 is the conductivity of insulator matrix (SDC); σ_1, dispersed electronic conductor (Ni); V, volume fraction of electronic conductor and n, experimental constant. The V_C corresponds to the volume fraction of electronic conductor at $(\sigma_1 + \sigma_0)/2$. The solid lines in Fig. 10 express Eq. (1) with $V_C = 21$ vol.% and $n = 1.3$ for Type A cermet and

with $V_C = 14$ vol.% and $n = 1.2$ for Type B cermet. This simulation apparently indicates the rapid decrease of resistance of Type B rather than Type A at a smaller fraction of Ni.

4. Conclusions

In this paper, the sinterability, microstructures and electrical properties of the following two types of Ni/Sm-doped ceria (SDC) cermet were studied: Type A-processed from mechanically mixed NiO and SDC powders with micrometer-sized porous secondary particles, Type B-processed by infiltrating $Ni(NO_3)_2$ solution into the SDC porous secondary particles and freeze-dried.

(1) Type B gave denser NiO/SDC secondary particles with high specific surface area than Type A because of the low reactivity between NiO and SDC primary particles mixed at nanometer scale. Increased NiO content reduced the specific surface area of the Type A powder but caused the increase of the specific surface area of Type B powder.
(2) Increased NiO content in Type A mixed powder reduced the sinterability. However, the relative density of Type B powder compact showed a maximum at 34 vol.% NiO (25 vol.% Ni).
(3) Sintered Type B compact offered a finer-grained microstructure than sintered Type A compact. In Type A cermet, Ni and SDC grains were mixed at intervals of 1–3 μm. More homogeneous distribution of Ni and SDC grains was measured in Type B cermet. That is, Type B cermet was superior to Type A cermet in achieving the high relative density, fine-grained microstructure and homogeneous distribution of Ni and SDC grains.
(4) NiO component in sintered Type A compact was easily reduced to Ni in the H_2/H_2O atmosphere at 700 °C. On the other hand, it took 24 h to reduce the NiO in sintered Type B compact to Ni in the H_2/H_2O atmosphere at 700 °C.
(5) The influence of Ni content on the electronic conductivity was small in the Ni content range from 20 to 100 vol.% for Type A cermet and of from 15 to 100 vol.% for Type B cermet. Both Types of Ni/SDC cermet showed the high stability of the low electronic resistance at 700 °C for 1–95 h in the H_2/H_2O atmosphere of oxygen partial pressure of 10^{-20} atm.

References

1. Minh, N. Q., Ceramic fuel cells. *J. Am. Ceram. Soc.* 1993, **76**, 563–588.
2. Jiang, S. P., Callus, P. J. and Badwal, S. P. S., Fabrication and performance of Ni/3 mol% Y_2O_3–ZrO_2 cermet anodes for solid oxide fuel cells. *Solid State Ionics* 2000, **132**, 1–14.
3. Dees, D. W., Claar, T. D., Easler, T. E., Fee, D. C. and Mrazek, F. C., Conductivity of porous Ni/ZrO_2–Y_2O_3 cermets. *J. Electrochem. Soc.* 1987, **134**, 2141–2146.
4. Nakagawa, N., Nakajima, K., Sato, M. and Kato, K., Contribution of the internal active three-phase zone of Ni-zirconia cermet anodes on the electrode performance of SOFCs. *J. Electrochem. Soc.* 1999, **146**, 1290–1295.
5. Pratihar, S. K., Basu, R. N. and Maiti, H. S., Preparation and characterization of porous Ni-YSZ cermet anode for solid oxide fuel cell application. *Trans. Indian Ceram. Soc.* 1997, **56**, 85–87.
6. Uchida, H., Suzuki, H. and Watanabe, M., High-performance electrode for medium-temperature solid oxide fuel cells. *J. Electrochem. Soc.* 1998, **145**, 615–620.
7. Eguchi, K., Ceramic materials containing rare earth oxides for solid oxide fuel cell. *J. Alloys Compd.* 1997, **250**, 486–491.
8. Livermore, S. J. A., Cotton, J. W. and Ormerod, R. M., Fuel reforming and electrical performance studies in intermediate temperature ceria-gadolinia-based SOFCs. *J. Power Sources* 2000, **86**, 411–416.
9. Zhang, X., Ohara, S., Maric, R., Mukai, K., Fukui, T., Yoshide, H. *et al.*, Ni-SDC cermet anode for medium-temperature solid oxide fuel cell with lanthanum gallate electrolyte. *J. Power Sources* 1999, **83**, 170–177.
10. Ohara, S., Maric, R., Zhang, X., Mukai, K., Fukui, T., Yoshide, H. *et al.*, High performance electrodes for reduced temperature solid oxide fuel cells with doped lanthanum gallate electrolyte I. Ni-SDC cermet anode. *J. Power Sources* 2000, **86**, 455–458.
11. Setoguchi, T., Okamoto, K., Eguchi, K. and Arai, H., Effects of anode material and fuel on anodic reaction of solid oxide fuel cells. *J. Electrochem. Soc.* 1992, **139**, 2875–2880.
12. Watanabe, M., Uchide, H., Shibata, M., Mochizuki, N. and Amikura, K., High performance catalyzed-reaction layer for medium temperature operating solid oxide fuel cells. *J. Electrochem. Soc.* 1994, **141**, 342–347.
13. Okawa, Y., Matsumoto, T., Doi, T. and Hirata, Y., Thermal stability of nanometer-sized NiO and Sm-doped ceria powders. *J. Mater. Res.* 2002, **17**, 2266–2274.
14. Higashi, K., Sonoda, K., Ono, H., Sameshima, S. and Hirata, Y., Surface properties and aqueous processing of rate earth-doped ceria powders by coprecipitation method. *Key Eng. Mater.* 1999, **159-160**, 25–30.
15. Higashi, K., Sonoda, K., Ono, H., Sameshima, S. and Hirata, Y., Synthesis and sintering of rate-earth-doped ceria powder by the oxalate coprecipitation method. *J. Mater. Res.* 1999, **14**, 957–967.
16. Kusy, R. P., Influence of particle size ratio on the continuity of aggregates. *J. Appl. Phys.* 1977, **48**, 5301–5304.
17. Malliaris, A. and Turner, D. T., Influence of particle size on the electrical resistivity of compacted mixtures of polymeric and metallic powders. *J. Appl. Phys.* 1971, **42**, 614–618.
18. Holm, E. A. and Cima, M. J., Two-dimensional whisker percolation in ceramic matrix-ceramic whisker composite. *J. Am. Ceram. Soc.* 1989, **72**, 303–305.
19. Kawaoka, H., Kim, Y.-H., Sekino, T., Choa, Y.-H., Kusunose, T., Nakayama, T. *et al.*, New approach to provide an electrical conductivity to structural ceramics. *J. Ceram. Proc. Res.* 2001, **2**, 1–3.
20. Mamunya, Y. P., Davidenko, V. V., Pissis, P. and Lebedev, E. V., Electrical and thermal conductivity of polymers filled with metal powders. *Eur. Polym. J.* 2002, **38**, 1887–1897.
21. Smith, D. P. and Anderson, J. C., Theory of electrical conduction in particulate systems. *Philos. Mag.* 1981, **43**, 797–798.
22. Mamunya, E. P., Davidenko, V. V. and Lebedev, E. V., Percolation conductivity of polymer composites filled with dispersed conductive filler. *Polym. Compos.* 1995, **16**, 319–324.
23. Mamunya, E. P., Davidenko, V. V. and Lebedev, E. V., Effect of polymer–filler interface interactions on percolation conductivity of thermoplastics filled with carbon black. *Compos. Interf.* 1997, **4**, 169–176.